NATIONAL AERONAUTICS AND SPACE ADMINISTRATION

Technical Report 32-1252

Radiation Mapping of a Planetary Surface Lander System

P. J. Gingo

JET PROPULSION LABORATORY

CALIFORNIA INSTITUTE OF TECHNOLOGY

PASADENA, CALIFORNIA

April 15, 1968

NATIONAL AERONAUTICS AND SPACE ADMINISTRATION

Technical Report 32-1252

Radiation Mapping of a Planetary Surface Lander System

P. J. Gingo

Approved by:

P. Goldsmith, *Manager*
Spacecraft Power Section

JET PROPULSION LABORATORY
CALIFORNIA INSTITUTE OF TECHNOLOGY
PASADENA, CALIFORNIA

April 15, 1968

Contents

Tables

Figures

Contents (contd)

Figures (contd)

Abstract

This report describes the radiation mapping analysis of a capsule lander system with three radioisotope thermoelectric generators for advanced space missions. The integration analysis, with the geometric model used to provide the radiation map, defines the radiation field produced by the power generators including the deorbit motor. Statistical data and graphs of the gamma dose rate and neutron flux provide the radiation intensities at numerous detection points to completely map the regions for the power generators and motor. These radiation intensity variances dictate careful location of each scientific instrument based on individual instrument characteristics.

Radiation Mapping of a Planetary Surface Lander System

I. Introduction

Radioisotope thermoelectric generators (RTG) are being evaluated as primary sources of electric power for advanced space missions where solar energy cannot provide the power required by the mission profile. On surface lander missions to the outer planets, the RTG appears to offer a favorable trade-off as a primary power source.

In the analysis of RTGs and their integration on the space vehicle, the potential radiation hazard presented by the radioisotope heat source must be defined. The radiation hazard can be a problem concerning handling safety, a component or subsystem degrading problem whereby the total radiation dose produces component degradation or damage, or an interference problem in which the radiation emitted by the heat source produces spurious counts in a scientific instrument that is part of the mission payload. It becomes paramount in the integration analysis to define the radiation field produced by the power generator so that these effects can be evaluated for a typical mission.

II. Radiation Analyses

During the course of planetary mission definition studies, a Mars soft lander having a roving capability was studied. Such a vehicle, shown in Fig. 1, could be carried to the Mars surface by a capsule bus that soft lands. After touchdown, the vehicle would be off-loaded to traverse short distances on the Martian surface to gather visual, geodetic, and life science data.

As shown in the figure, three RTGs, each generating 2600 thW (150 eW), could be used to provide power for the vehicle operation. This vehicle, with the generators located as shown in the figure, was considered to be typical and was used to define the radiation flux and dose levels generated as a result of using plutonium dioxide as a fuel source. The resulting radiation map is to be used to determine what effects can be expected on equipment and components located within the vehicle and its attendant radiation field.

A. Surface Lander Geometry

The geometric model used for the radiation mapping was selected primarily to provide a radiation map for the region above, below, and between the RTGs. This region is needed to locate the scientific instruments, therefore, it must be completely mapped. The gamma dose rates and neutron fluxes at each detector point were calculated as the numerical sum of the gamma dose rates and neutron fluxes generated by each RTG.

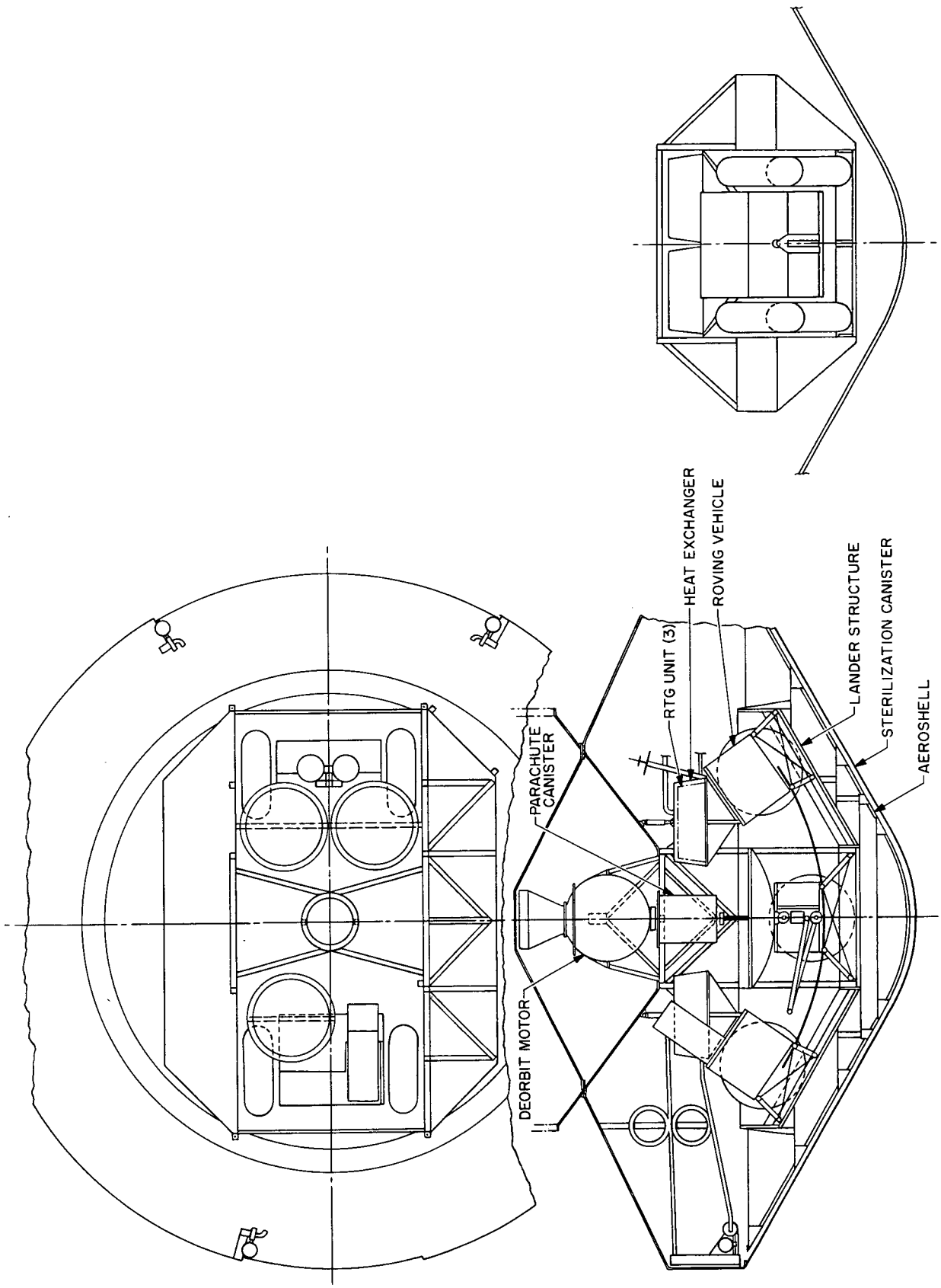

Fig. 1. Roving soft lander system

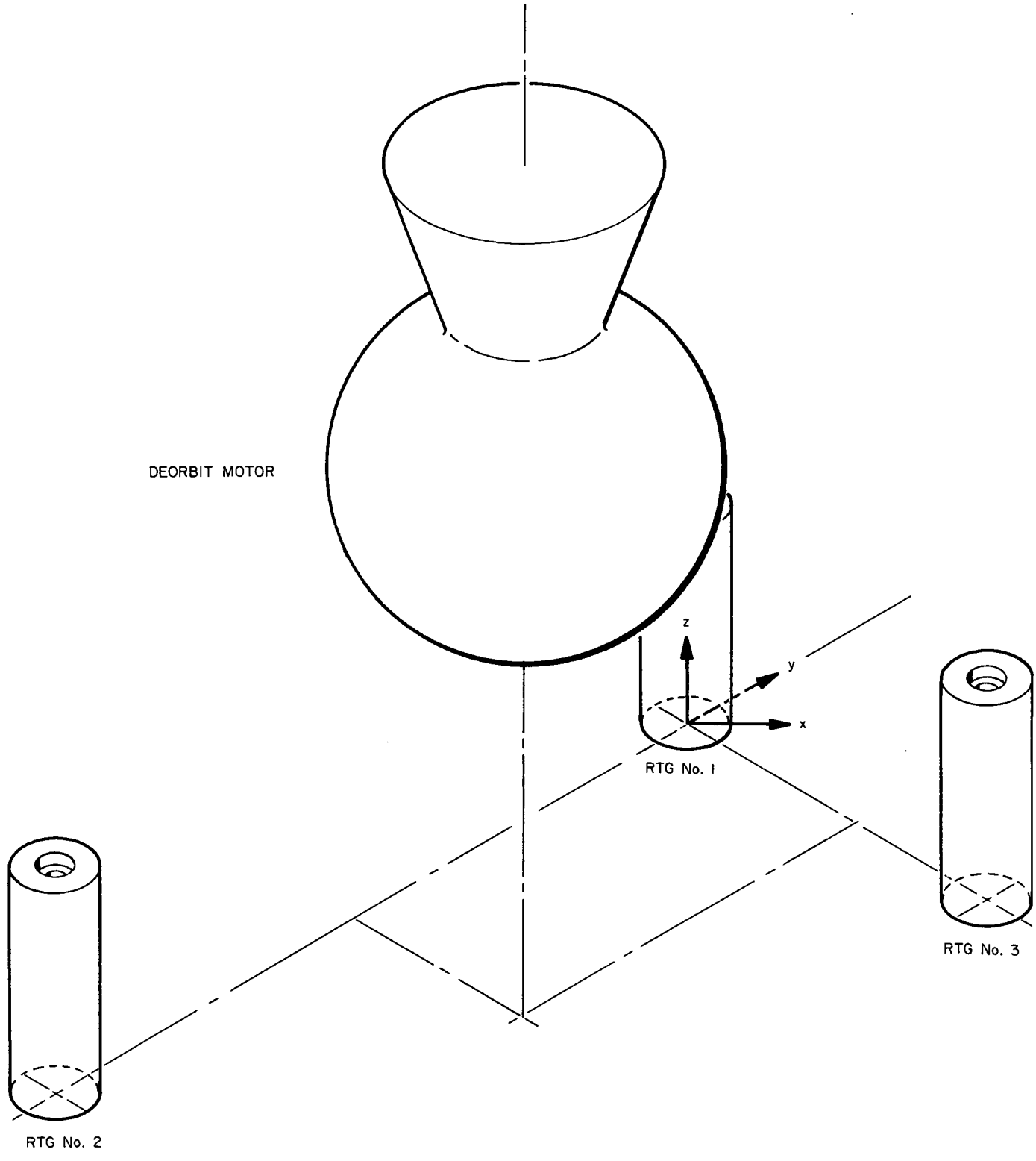

Fig. 2. Geometric model and cartesian coordinate origin

The geometric model and the cartesian coordinate origin used for the radiation analysis is shown in Fig. 2. The RTG labeled No. 1 was used as the source of the neutrons and gammas emitted by the plutonium dioxide fuel described in Ref. 1. The RTG No. 1 was placed on the coordinate $r = 0$ cm, $\theta = 0$ deg, and $z = 0$ cm; the RTG No. 2 was placed on the coordinate $r = 166.7$ cm, $\theta = 180$ deg, and $z = 0$ cm; and the RTG No. 3 was placed on the coordinate $r = 79.4$ cm, $\theta = 270$ deg, and $z = 0$ cm. The center of the deorbit motor was placed on the coordinate $r = 89.9$ cm, $\theta = 263°33'7''$, and $z = 106.6$ cm.

The neutron and gamma rays emanating from RTG No. 1 are attenuated by the other two RTGs only for emission angles of 180 and 270 deg, respectively. This attenuation will be referred to as the self-attenuated beams. The detector points in the plane above the deorbit motor are attenuated by the deorbit motor for emission angle of 263° 33′ 7″. The neutron and gamma radiations from the RTG No. 1 have been combined with the self-attenuated beams and the deorbit motor attenuation factors to determine the gamma dose rate and neutron fluxes produced by the three RTGs.

The radioisotope fuel generator selected for the study consists of the following regions, proceeding radially from the central void region and continuing to the outermost region (cladding).

(1) The central void region is required to contain the gases generated by the decay of the fissionable fuels.

(2) The second interior region is a Haynes 25 alloy clad (0.051-cm thick).

(3) The third interior region contains the plutonium dioxide fuel.

(4) The fourth interior region is a Haynes 25 alloy clad (0.051-cm thick).

(5) The final or outermost region contains the thermoelectric generator elements, which are assumed to be homogeneous in this region.

The construction of the radioisotope thermoelectric generator is shown in Fig. 3. The void volume was assumed to extend axially to each end of the generator. This assumption does not affect either the material attenuation or the geometric attenuation factors in the axial direction.

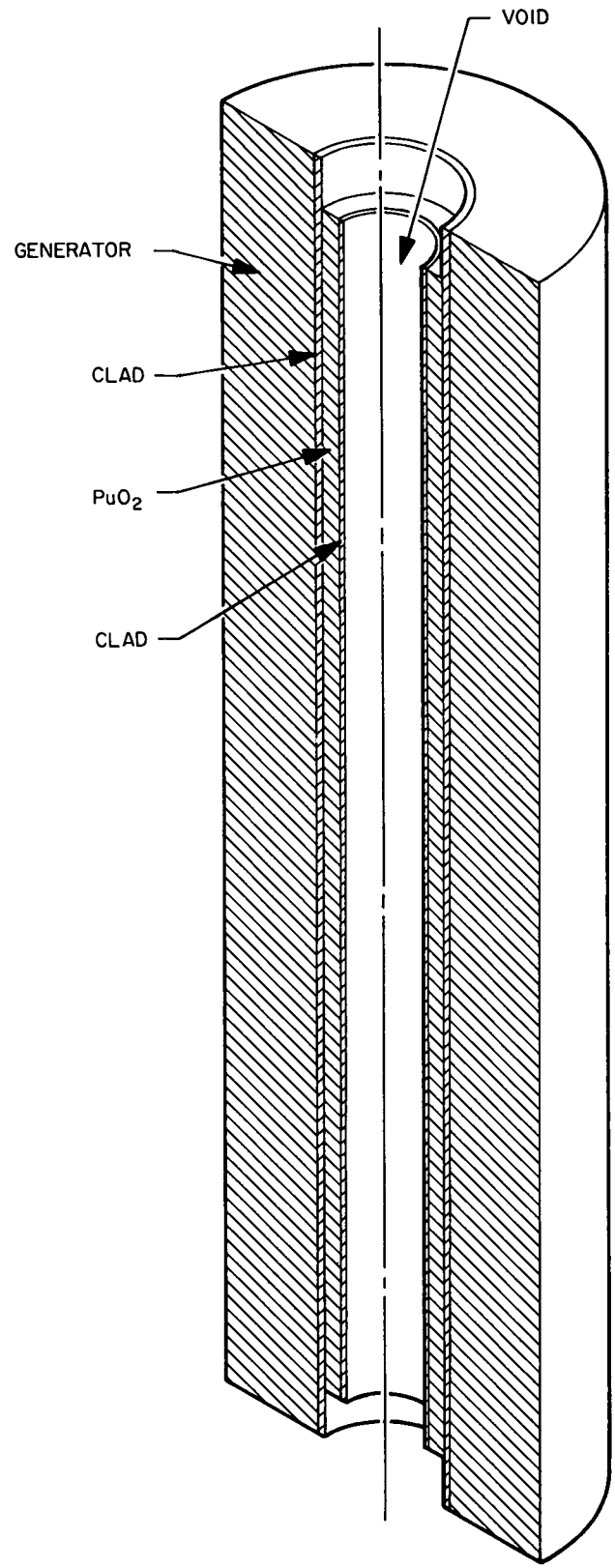

Fig. 3. Radioisotope thermoelectric generator, sectional diagram

B. Analytical Method

This study was made with a version of "QAD B," a Los Alamos Scientific Laboratory originated shielding program which utilizes the point kernel source and ray tracing technique to determine the dose rate at a given detector point.

The method involves representing the source volumes by a number of subdivided volume elements considered as kernels or points radiating isotropically. The distances through all regions or materials is traversed as a narrow radiation beam in a line-of-sight ray from the source points to the desired dose point or receptor point. From the distances travelled through the regions and the attenuation characteristics of the materials in these regions, energy-dependent attenuation coefficients and an energy-dependent buildup factor are applied to calculate the suitable gamma dose rate at the desired detector point. The gamma ray buildup factors are determined for a single material (tin was used in this study) that represents all materials within the given regions. The buildup factors increased the incident dose rate or particle flux due to multiple scattering and nonisotropic scattering in regions outside of the assumed line-of-sight ray.

After the application of the suitable conversion factors, the desired responses, such as dose rate, energy deposition, or particle flux to the radiation from the individual source points, are summed into a total source energy group.

For the neutron attenuation calculation, the QAD B uses a modified Albert-Welton kernel. A complex exponential function is empirically fitted to the experimental data. The data consist of measured attenuation of neutrons through slabs of the given materials that are placed in an infinite water medium. The neutron material attenuation is determined by a neutron single-energy removal cross section.

The QAD B source was corrected from the assumed ^{235}U source to correspond to the PuO_2 source strength used in this study. The QAD B neutron spectrum was assumed to apply for the plutonium dioxide fuel, however, the total neutron fission yield was reduced from 7.63×10^{10} neutrons/W-s (this value applied to ^{235}U) to 5.18×10^{4} neutrons/W-s, which, in turn, applied to the presently considered PuO_2 product fuel. If the assembly were critical, 3.3×10^{10} neutrons/W-s normally would be available for leakage in the ^{235}U fuel.

1. Gamma kernel. For each source energy group i, the gamma dose rate is computed as a point kernel radiating isotropically and is numerically summed throughout the complete source region:

$$D_{u\gamma_i} = \sum_{\substack{l=1 \\ m=1 \\ n=1}}^{L,M,N} \frac{E_i K_i S_{l,m,n} \epsilon^{-X_i}}{4\pi\rho^2_{S_{l,m,n}}} \tag{1}$$

where

$$X_i = \sum_{M_o=1}^{M_o} \sum_{h=1}^{H} \rho_h \theta_{m_o h} \Sigma_{m_o i} \tag{2}$$

is the macroscopic attenuation coefficient consistent with each (l, m, n) source point, and the h^{th} composition of material m_o within the source energy group i.

2. Gamma buildup factor. Using the gamma buildup factor, the response of the detector located at the receptor point is given as:

$$D_{\gamma_i} = B_i D_{u\gamma_i} \tag{3}$$

with $D_{u\gamma_i}$ as the narrow beam line-of-sight ray proceeding from sources to detector. The buildup factor must be consistent with the units of the uncollided dose rate, i.e., buildup factor for dose rate, or energy deposition.

The buildup factor applied to the uncollided flux to obtain the total response within an energy group is:

$$B_i = \beta_0 + \beta_1 X_i + \beta_2 X_i^2 + \beta_3 X_i^3 \tag{4}$$

The normal polynomial approximation of gamma ray buildup factors and the normal gamma absorption coefficients were used in this study.

3. Neutron kernel. The QAD B provides an estimate of the neutron dose rates by using a modification of the Albert-Welton kernel.

$$D_\alpha = \frac{S\beta}{4\pi\rho^2_{S_{l,m,n}}} \tag{5}$$

where

$$\beta = \alpha_1 y^{\alpha_2} \exp\left[-\alpha_3 y^{\alpha_4} \exp\left(- \sum_{m_o=1}^{M_o} \sum_{h=1}^{H} \rho_h \theta_{m_o h} \Sigma_{m_o} \right) \right] \tag{6}$$

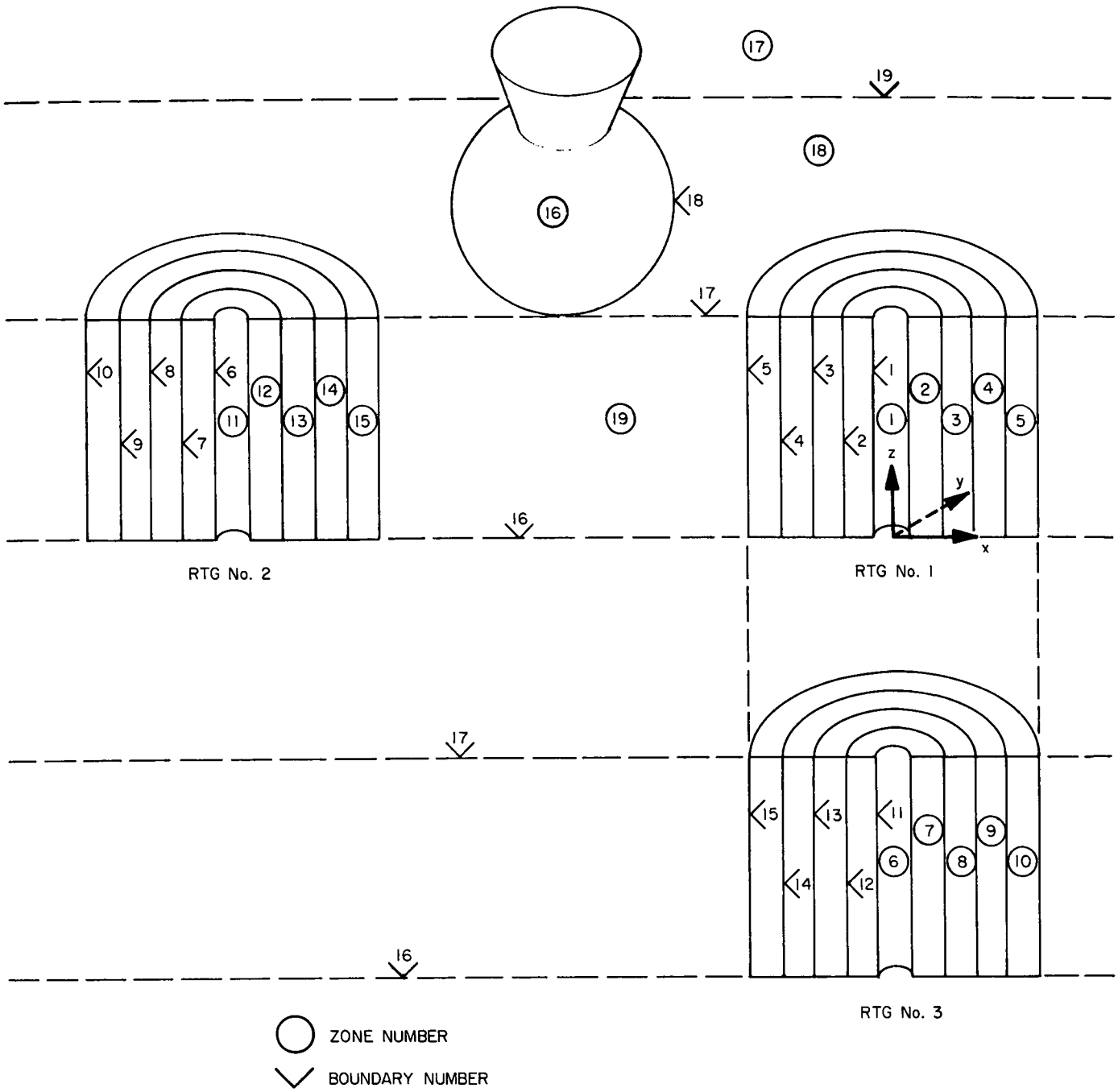

Fig. 4. Zone and boundary definitions

and

$$y = \sum_{m_o=1}^{M_o} \sum_{h=1}^{H} \rho_h \theta_{m_o h} X_{m_o} \qquad (7)$$

The QAD B values selected for the empirical fits are:

$$\alpha_1 = 3.915 \times 10^{-9}$$

$$\alpha_2 = 0.29 \times 10^{0}$$

$$\alpha_3 = 0.83 \times 10^{0}$$

$$\alpha_4 = 0.58 \times 10^{0}$$

The empirical constants should be adjusted to fit measured neutron dose rates from different radioisotope fuels. Neutron removal cross sections were taken from Ref. 2.

Table 1. Surface lander system zone and boundary parameters

Zone	Parameter[a]											
	B_o	h	$j \cdot \lambda_1$	P_1	$j \cdot \lambda_2$	P_2	$j \cdot \lambda_3$	P_3	$j \cdot \lambda_4$	P_4	$j \cdot \lambda_5$	P_5
1	3	1	17	18	−16	20	1	2	—	—		
2	4	2	17	18	−16	20	2	3	−1	1		
3	4	3	17	18	−16	20	3	4	−2	2		
4	4	2	17	18	−16	20	4	5	−3	3		
5	4	4	17	18	−16	20	5	19	−4	4		
6	3	1	17	18	−16	20	11	7	—	—		
7	4	2	17	18	−16	20	12	8	−11	6		
8	4	3	17	18	−16	20	13	9	−12	7		
9	4	2	17	18	−16	20	14	10	−13	8		
10	4	4	17	18	−16	20	15	19	−14	9		
11	3	1	17	18	−16	20	6	12	—	—		
12	4	2	17	18	−16	20	7	13	−6	11		
13	4	3	17	18	−16	20	8	14	−7	12		
14	4	2	17	18	−16	20	9	15	−8	13		
15	4	4	17	18	−16	20	10	19	−9	14		
16	1	5	18	18	—	—	—	—	—	—		
17	−1	1	−19	18	—	—	—	—	—	—		
18	3	1	19	17	−17	19	−18	16	—	—		
19	5	1	17	18	−16	20	−10	15	−5	5	−15	10
20	−1	1	−16	19	—	—	—	—	—	—		

[a] B_o = number of boundaries for given zone (− indicates outside zone and + indicates inside zone), h = composition number, λ = boundary number, j = direction index, and P = zone number.

C. Surface Lander Geometry Input Data

The various regions and the corresponding boundaries that designates each region are defined by the region or zone numbers and the boundary numbers in Fig. 4. The QAD B zone and boundary parameters used for this study are listed in Table 1. The material densities occupying each region are given in Table 2, and the atomic densities of the very same materials are given in Table 3. The atomic densities were used only to verify the material densities in each region.

The method of calculation is shown in Table 4. Each surface used to bound the given regions have equations that correspond to the base of RTG No. 1, given in Fig. 2.

The gamma ray source strength and the conversion from photon flux to photon dose are given in Table 5. This table was reduced from Table 6, which gives more extensive dose rate conversion factors.

III. Final Results

The completed attenuated gamma dose rates and neutron fluxes are plotted and presented in Figs. 5–11. The gamma dose rates and neutron fluxes were plotted from the calculated radiation intensity values given in Table 7. The gamma dose rates and neutron fluxes in Figs. 5 and 7, respectively, have been given for detector points located in the various planes that are most representative as useful planes to completely map the region for the RTGs and motor. The plane $z = 25$ cm passes through the middle of each RTG and will have the maximum radial dose rates. The plane $z = 50$ cm that has the very same radiation dose rates as the base plane $z = 0$ cm represents the beginning of the transition region from radial detector points to axial detector points. The various planes up to $z = 100$ cm are below the deorbit motor while the planes $z = 100$, 120, and 150 cm have been included to determine the dose rates attenuated by the deorbit motor.

The gamma dose rates and neutron fluxes attenuated by the remaining RTGs and the deorbit motor are plotted in Figs. 6 and 8, respectively. The dose rates given in Figs. 5–8 were combined to produce the isodose curves in Figs. 9 and 10 and the isoflux curves in Fig. 11. These contour curves were generated in the following manner: each detector point was identified in terms of the three radial coordinates from each RTG. The dose rate or flux was determined for each radial coordinate and summed for the three radial coordinates for each detector point.

Table 2. Material densities[a]

Zone	Description	Material, g/cm³																
		Co	Cr	Ni	W	Mn	Fe	Be	Pb	Cu	N_2	H_2	Cl	O_2	C	^{238}Pu	^{239}Pu	^{240}Pu	^{241}Pu
1	Void																		
2	RTG: clad	4.7985	1.828	0.914	1.371	0.1371	0.0914												
3	RTG: fuel	—	—	—	—	—	—	—	—	—	—	—	—	0.8877	—	5.3677	0.9945	0.1931	0.05349
4	RTG: clad	4.7985	1.828	0.914	1.371	0.1371	0.0914												
5	RTG: thermo-element	—	0.0748	—	—	—	0.4920	0.8543	2.5776	0.3768									
6	Void																		
7	RTG: clad	4.7985	1.828	0.914	1.371	0.1371	0.0914												
8	RTG: fuel	—	—	—	—	—	—	—	—	—	—	—	—	0.8877	—	5.3677	0.9945	0.1931	0.05349
9	RTG: clad	4.7985	1.828	0.914	1.371	0.1371	0.0914												
10	RTG: thermo-element	—	0.0748	—	—	—	0.4920	0.8543	2.5776	0.3768									
11	Void																		
12	RTG: clad	4.7985	1.828	0.914	1.371	0.1371	0.0914												
13	RTG: fuel	—	—	—	—	—	—	—	—	—	—	—	—	0.8877	—	5.3677	0.9945	0.1931	0.05349
14	RTG: clad	4.7985	1.828	0.914	1.371	0.1371	0.0914												
15	RTG: thermo-element	—	0.0748	—	—	—	0.4920	0.8543	2.5776	0.3768									
16	Propellant[b]	—	—	—	—	—	—	—	—	—	0.0874	0.0279	0.22106	0.3991	0.01644				
17	Void																		
18	Void																		
19	Void																		
20	Void																		

[a]Material density for each zone was calculated as follows: zone material density = weight fraction × material density.

[b]Propellant used was carboxy terminated polybutadiene (CTPB) composite of 82% NH_4ClO_4 + 18% CH_2.

Table 3. Atomic densities[a]

Zone	Description	Material, atoms/cm^3 × 10^{24}																	
		Co	Cr	Ni	W	Mn	Fe	Be	Pb	Cu	N_2	H_2	Cl	O_2	C	^{238}Pu	^{239}Pu	^{240}Pu	^{241}Pu
1	Void																		
2	RTG: clad	0.04902	0.02115	0.0094	0.00448	0.0015	0.00098												
3	RTG: fuel	—	—	—	—	—	—	—	—	—	—	—	—	0.02984	—	0.01208	0.00223	0.00042	0.00011
4	RTG: clad	0.04902	0.02115	0.0094	0.00448	0.0015	0.00098												
5	RTG: thermo-element	—	0.00076	—	—	—	0.00541	0.0571	0.00749	0.00357									
6	Void																		
7	RTG: clad	0.04902	0.02115	0.0094	0.00448	0.0015	0.00098												
8	RTG: fuel	—	—	—	—	—	—	—	—	—	—	—	—	0.02984	—	0.01208	0.00223	0.00042	0.00011
9	RTG: clad	0.04902	0.02115	0.0094	0.00448	0.0015	0.00098												
10	RTG: thermo-element	—	0.00076	—	—	—	0.00541	0.0571	0.00749	0.00357									
11	Void																		
12	RTG: clad	0.04902	0.02115	0.0094	0.00448	0.0015	0.00098												
13	RTG: fuel	—	—	—	—	—	—	—	—	—	—	—	—	0.02984	—	0.01208	0.00223	0.00042	0.00011
14	RTG: clad	0.04902	0.02115	0.0094	0.00448	0.0015	0.00098												
15	RTG: thermo-element	—	0.00076	—	—	—	0.00541	0.0571	0.00749	0.00357									
16	Propellant[b]	—	—	—	—	—	—	—	—	—	0.00675	0.0518	0.00675	0.0270	0.01241				
17	Void																		
18	Void																		
19	Void																		
20	Void																		

[a]Atomic density for each element was calculated as follows: atomic density = mass density × volume fraction × (Avogadro No./at. wt).

[b]Propellant is CTPB containing 82% NH_4ClO_4 + 18% CH_2.

Table 4. Boundary (surface lander system surface) equations

Boundary	Equation	K	x_o	y_o	z_o
1	$(x - x_o)^2 + (y - y_o)^2 - K = 0$	2.920681	0	0	
2		3.0976	0	0	
3		8.86253	0	0	
4		9.16879	0	0	
5		53.50923	0	0	
6		2.920681	−166.6875	0	
7		3.0976	−166.6875	0	
8		8.86253	−166.6875	0	
9		9.16879	−166.6875	0	
10		53.50923	−166.6875	0	
11		2.920681	0	−79.375	
12		3.0976	0	−79.375	
13		8.86253	0	−79.375	
14		9.16879	0	−79.375	
15	$(x - x_o)^2 + (y - y_o)^2 - K = 0$	53.50923	0	−79.375	
16	$z - K = 0$	0	—	—	
17	$z - K = 0$	49.45	—	—	
18	$(x - x_o)^2 + (y - y_o)^2 + (z - z_o)^2 - K = 0$	1444	−80.645	−39.6875	106.6
19	$z - K = 0$	144.7	—	—	

Table 5. Plutonium dioxide gamma ray source intensities[a]

Energy group, MeV	Average energy, MeV	Source density, MeV/s/W	Photon flux to dose conversion, (rad/h)/(MeV/cm²-s)
0.04 - 0.5	0.2	1.078×10^{8}	1.69×10^{-6}
0.5 - 1.0	0.8	9.85×10^{5}	1.8×10^{-6}
1.0 - 2.0	1.5	19.2×10^{3}	1.6×10^{-6}
2.0 - 3.0	2.5	60.3×10^{3}	1.4×10^{-6}
3.0 - 5.0	4.0	14.4×10^{2}	1.2×10^{-6}
5.0 - 7.0	6.0	35.5×10^{0}	1.055×10^{-6}

[a]Data source; calculated for elapsed time, $t = 1$ yr from production.

Table 6. Dose rate conversion[a]

E, MeV	Conversion factor	E, MeV	Conversion factor
0.01	3.38×10^{-6}	1.5	2.40×10^{-6}
0.015	1.40×10^{-6}	2.0	2.76×10^{-6}
0.02	7.75×10^{-7}	2.5	3.50×10^{-6}
0.03	3.34×10^{-7}	2.8	3.70×10^{-6}
0.04	1.92×10^{-7}	3.0	3.93×10^{-6}
0.05	1.40×10^{-7}	3.5	4.30×10^{-6}
0.06	1.23×10^{-7}	4.0	4.79×10^{-6}
0.08	1.53×10^{-7}	4.5	5.20×10^{-6}
0.10	1.49×10^{-7}	5.0	5.57×10^{-6}
0.15	2.37×10^{-7}	5.5	6.0×10^{-6}
0.20	3.38×10^{-7}	6.0	6.33×10^{-6}
0.30	5.50×10^{-7}	6.5	6.70×10^{-6}
0.40	7.39×10^{-7}	7.5	7.50×10^{-6}
0.50	9.27×10^{-7}	8.0	7.79×10^{-6}
0.60	1.10×10^{-6}	8.5	8.30×10^{-6}
0.70	1.26×10^{-6}	9.5	9.50×10^{-6}
0.80	1.44×10^{-6}	10.0	9.76×10^{-6}
1.0	1.76×10^{-6}		

[a](rad/h)/(photons/cm²-s).

The neutron flux to dose conversion has been averaged to a value of 0.1169 mrem/h/neutrons/cm²-s. This average conversion factor has been calculated for the neutron group structure used in QAD B.

IV. Conclusions

As a result of this study, the degradation of the selected science instruments used in this capsule landed system can be related to the expected dose rates from the three 2600-thW radioisotope thermoelectric generators. In addition, if Figs. 9 and 11 are used as radiation maps for the RTG system, the following conclusions are reached.

(1) The radioisotope thermoelectric generator is primarily a neutron emitter. In Fig. 11, the isodose curve, 1.1×10^{-5} rad/h-thW, corresponds to a total dose rate of 0.03 rad/h. In Fig. 9, the neutron isoflux curve, 2 neutrons/cm²-s-thW, corresponds to a total dose rate of 6 rem/h.

This neutron isoflux 2.0 curve region of Fig. 9 will then yield a neutron to gamma dose rate ratio of approximately 30 to 1. A normally quoted value of the bare capsule neutron to gamma dose rate is 5 to 1. This increase is due to the presence of the heavy elements in the generator producing a greater attenuation for the gamma rays.

The neutron dose rate at the surface of RTG No. 1 is approximately 15 rem/h while the surface gamma dose rate is approximately 0.50 rad/h. Although the intensity levels increased by a factor of 2.5, the ratio of the neutron to gamma dose rate still remains at 30 to 1.

(2) The total dose rates expected in this vehicle can vary considerably depending upon the detector location. This variance will mean some scientific instruments, which are marginally operational in the radiation field near the RTGs, must be located more carefully on the basis of the characteristics of each instrument.

(3) The total surface dose rates of 15 rem/h are moderate dose rates; but for missions involving long periods of irradiation, the expected dose rates must be determined more precisely, including the spectral components.

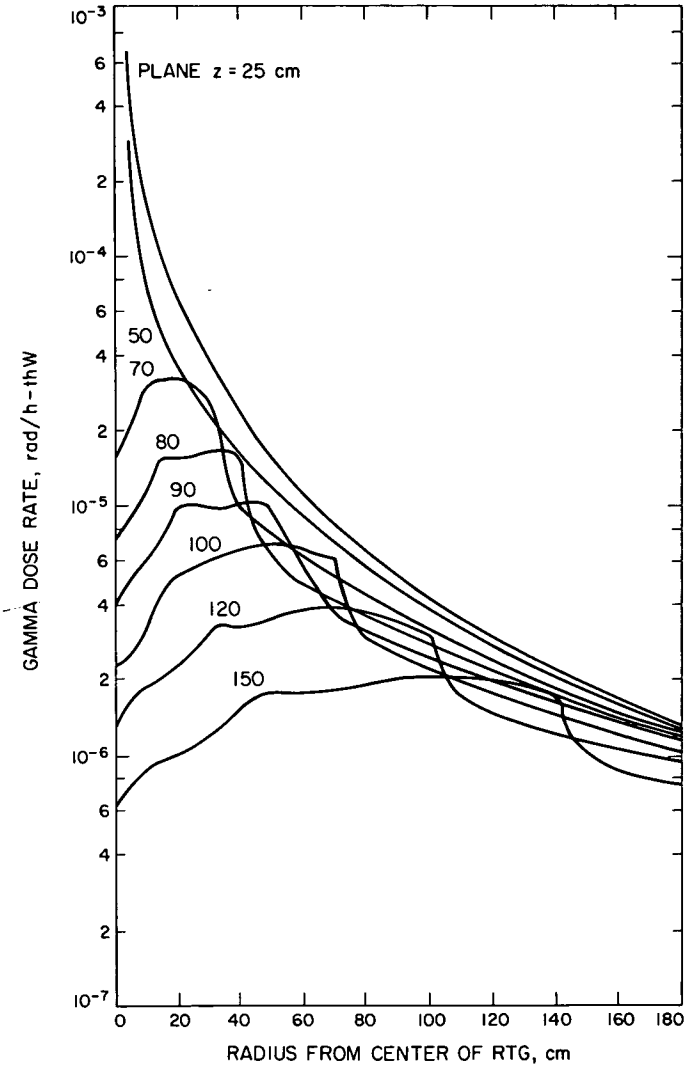

Fig. 5. Gamma dose rate for single capsule

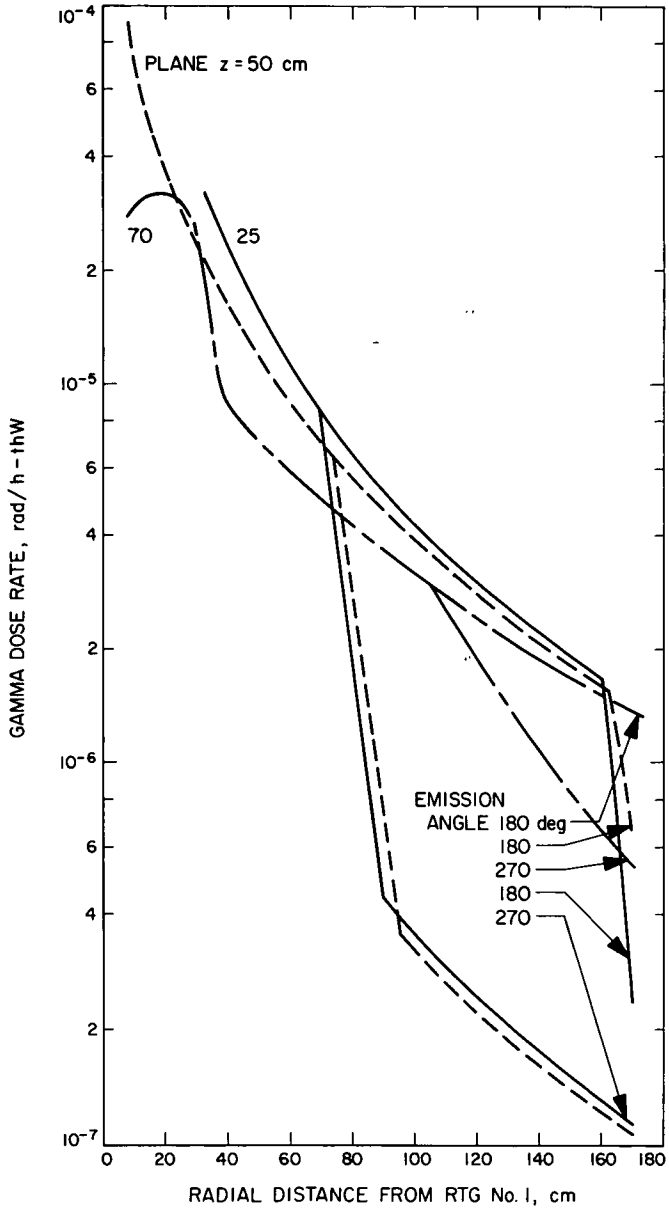

Fig. 6. Gamma dose rate vs emission angle from RTG No. 1

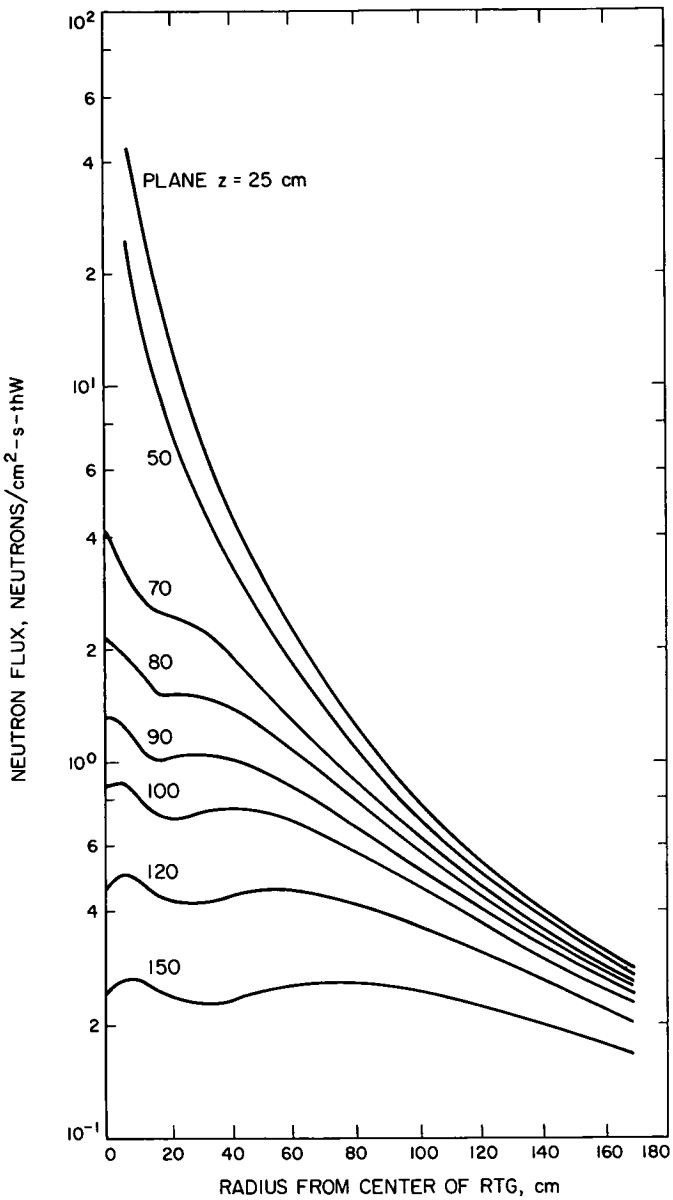

Fig. 7. Neutron flux for single capsule

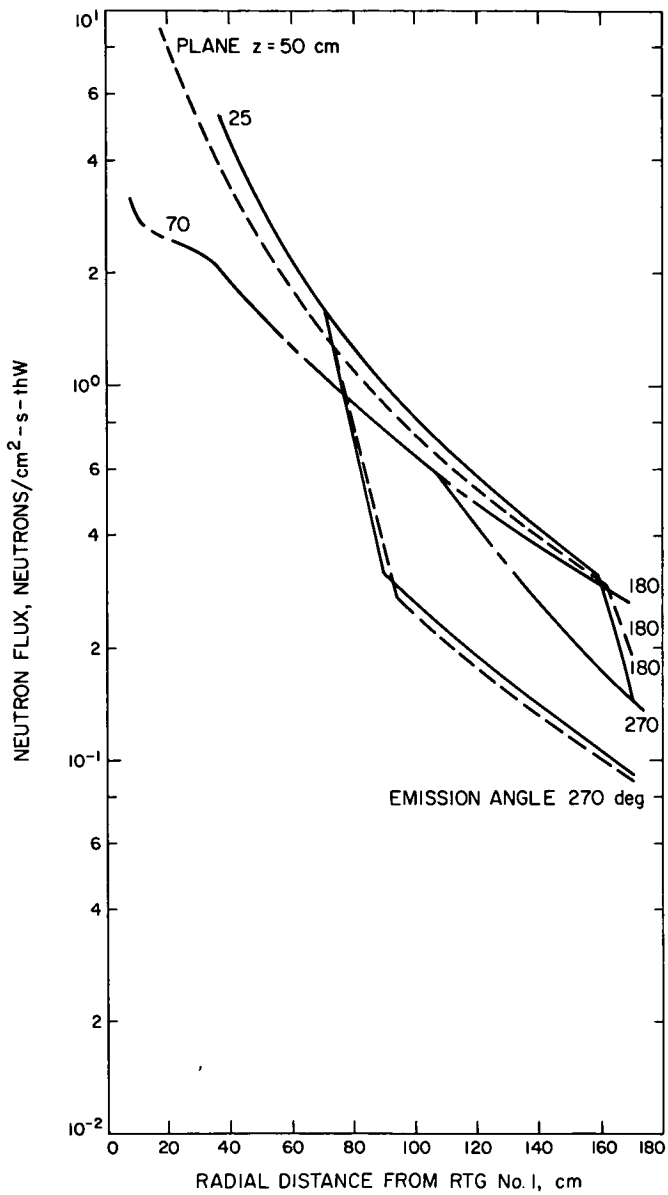

Fig. 8. Neutron flux vs emission angle from RTG No. 1

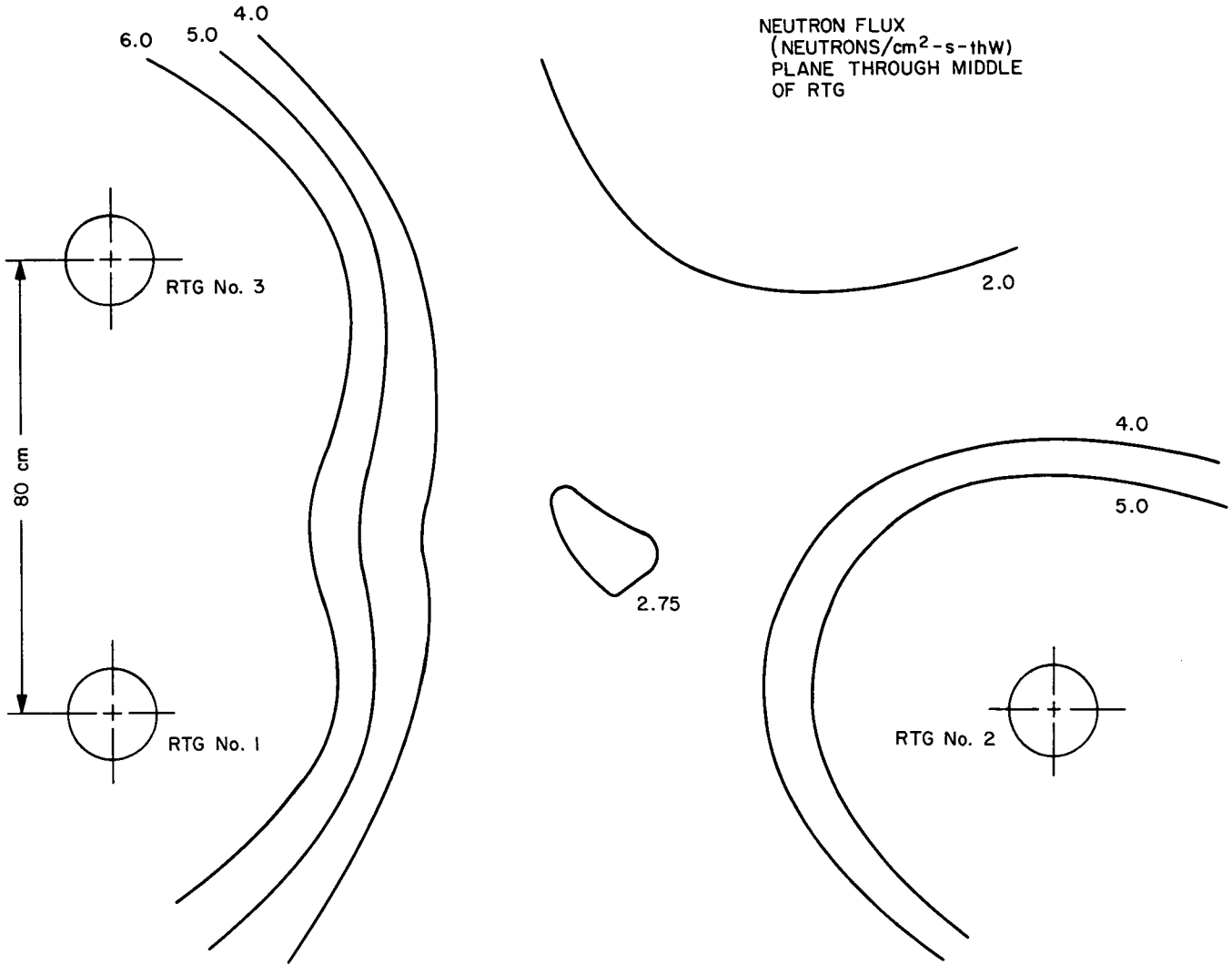

Fig. 9. Isodose curves of neutron flux

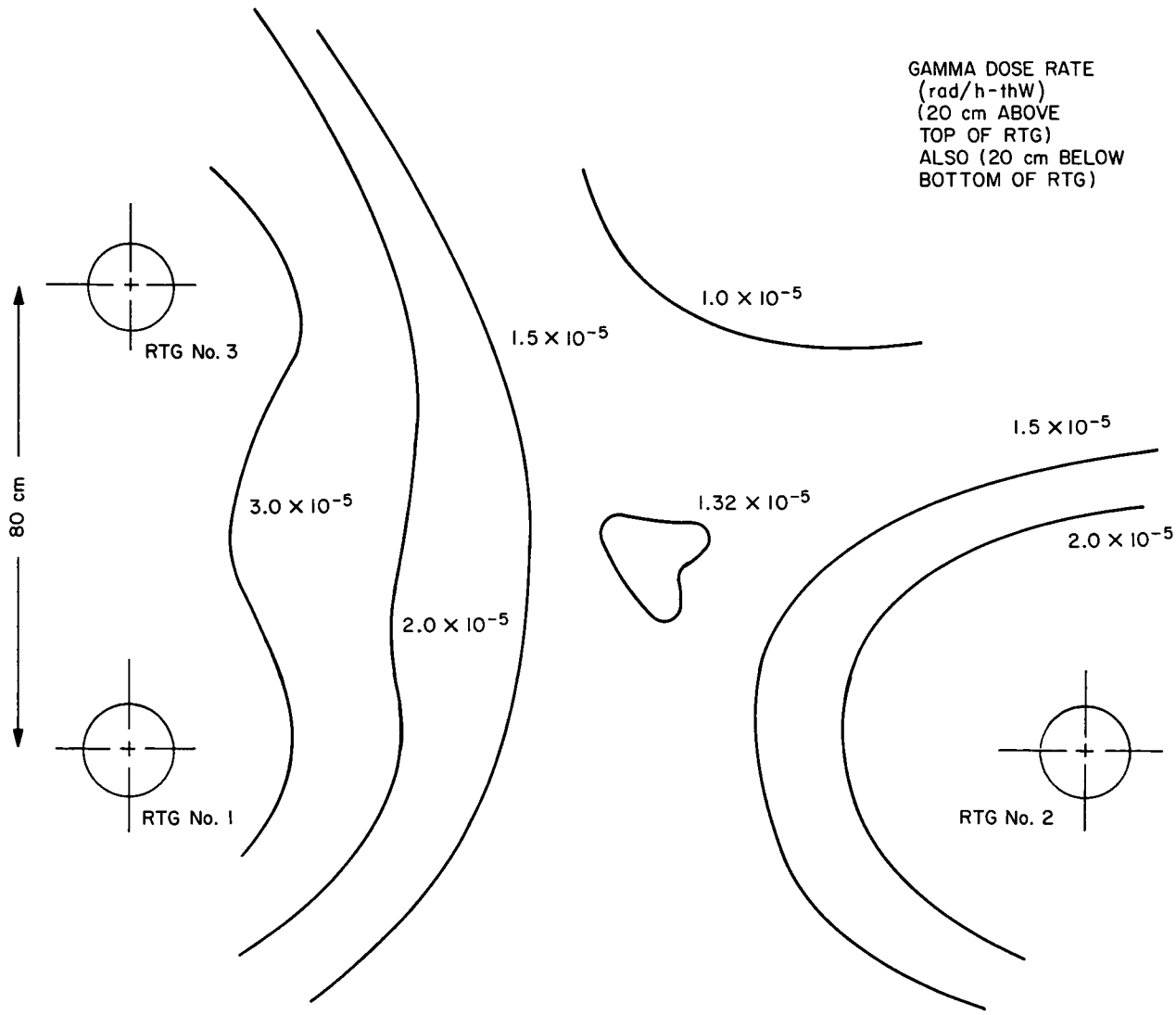

Fig. 10. Isodose curves of gamma dose rate

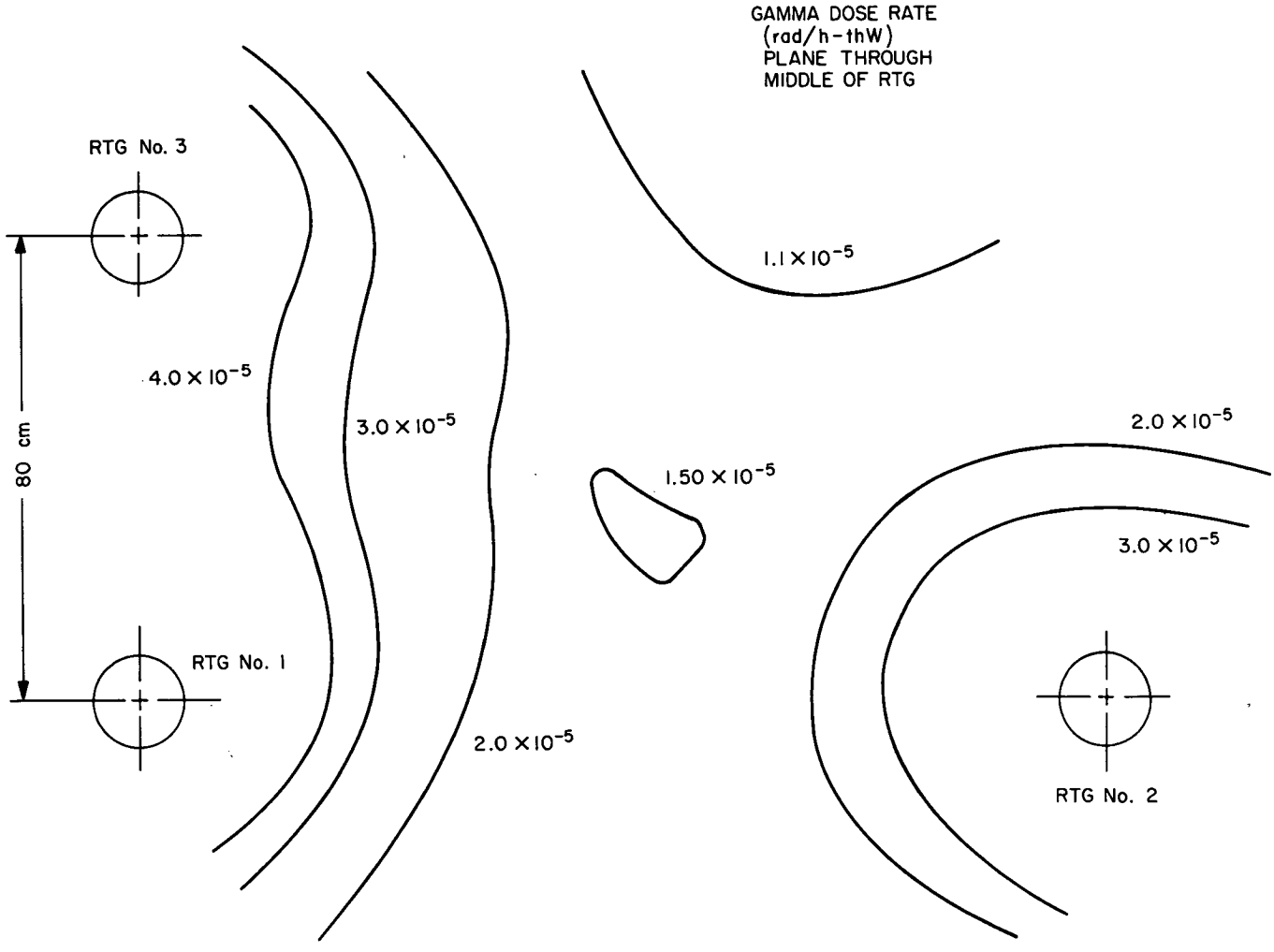

Fig. 11. Isoflux curves of gamma dose rate

Table 7. Plutonium dioxide radioisotope radiation intensities

Coordinates		Radiation intensity	
Radius, cm	Angle, deg	Gamma dose rate, rad/h-thW	Neutron flux, neutrons/cm^2-s-thW
Plane z = 25 cm			
0	0, 90	1.8279×10^{-2}	1.3223×10^{2}
4		6.66×10^{-4}	1.0932×10^{2}
8		1.8571×10^{-4}	4.3172×10^{1}
40		2.2910×10^{-5}	4.489×10^{0}
90		5.174×10^{-6}	0.9791×10^{0}
120		2.9567×10^{-6}	0.5574×10^{0}
140		2.184×10^{-6}	0.41118×10^{0}
170		1.4882×10^{-6}	0.2799×10^{0}
8	180	1.8571×10^{-4}	4.3172×10^{1}
40		2.2910×10^{-5}	4.489×10^{0}
90		5.174×10^{-6}	0.9791×10^{0}
120		2.9567×10^{-6}	0.5574×10^{0}
140		2.184×10^{-6}	0.41118×10^{0}
150		1.9061×10^{-6}	0.35871×10^{0}
160		1.5151×10^{-6}	0.3057×10^{0}
163		8.9453×10^{-7}	0.23046×10^{0}
168		4.2977×10^{-7}	0.17717×10^{0}
170		2.332×10^{-7}	0.1459×10^{0}
8	270	1.8571×10^{-4}	4.3172×10^{1}
40		2.291×10^{-5}	4.489×10^{0}
45		1.8702×10^{-5}	3.634×10^{0}
50		1.5522×10^{-5}	2.9975×10^{0}
60		1.1141×10^{-5}	2.1323×10^{0}
70		8.3566×10^{-6}	1.5909×10^{0}
80		1.8032×10^{-6}	0.75364×10^{0}
90		4.3063×10^{-7}	0.3055×10^{0}
120		2.4005×10^{-7}	0.1891×10^{0}
140		1.7303×10^{-7}	0.1381×10^{0}
170		1.1341×10^{-7}	0.09245×10^{0}
Plane z = 50 cm			
0	0, 90	5.2979×10^{-3}	5.7944×10^{1}
4		2.7885×10^{-4}	4.6078×10^{1}
8		8.9615×10^{-5}	2.0788×10^{1}
20		3.4992×10^{-5}	8.0444×10^{0}
40		1.5927×10^{-5}	3.3887×10^{0}
60		8.9872×10^{-6}	1.819×10^{0}
90		4.6243×10^{-6}	0.9033×10^{0}
120		2.7639×10^{-6}	0.5311×10^{0}
140		2.076×10^{-6}	0.3966×10^{0}
170		1.4368×10^{-6}	0.2730×10^{0}
8	180	8.9615×10^{-5}	2.0788×10^{1}
20		3.4992×10^{-5}	8.0444×10^{0}
40		1.5927×10^{-5}	3.3887×10^{0}
60		8.9872×10^{-6}	1.8190×10^{0}
90		4.6243×10^{-6}	0.9033×10^{0}
120		2.7639×10^{-6}	0.5311×10^{0}
140		2.076×10^{-6}	0.3966×10^{0}
163		1.428×10^{-6}	0.286×10^{0}
166		1.0473×10^{-6}	0.2381×10^{0}
168		7.7811×10^{-7}	0.2085×10^{0}
170		6.622×10^{-7}	0.1936×10^{0}
8	270	8.9615×10^{-5}	2.0788×10^{1}
20		3.4992×10^{-5}	8.0444×10^{0}
40		1.5927×10^{-5}	3.3887×10^{0}
60		8.9872×10^{-6}	1.8190×10^{0}
72		6.7352×10^{-6}	1.3389×10^{0}
75		5.3753×10^{-6}	1.1549×10^{0}
80		2.3627×10^{-6}	0.7477×10^{0}
90		7.5405×10^{-7}	0.3641×10^{0}
120		2.157×10^{-7}	0.1748×10^{0}
140		1.5954×10^{-7}	0.1302×10^{0}
170		1.0716×10^{-7}	0.0888×10^{0}
Plane z = 70 cm			
0	0, 90	1.5564×10^{-5}	4.1138×10^{0}
4		1.929×10^{-5}	3.5829×10^{0}
6		2.2873×10^{-5}	3.2860×10^{0}
8		2.7223×10^{-5}	3.0724×10^{0}
15		3.1749×10^{-5}	2.5662×10^{0}
20		3.2089×10^{-5}	2.4738×10^{0}
25		3.0327×10^{-5}	2.3886×10^{0}
30		2.7079×10^{-5}	2.2639×10^{0}
40		8.5245×10^{-6}	1.9501×10^{0}
90		3.6648×10^{-6}	0.7638×10^{0}
120		2.3972×10^{-6}	0.4799×10^{0}
140		1.8634×10^{-6}	0.3672×10^{0}
170		1.3323×10^{-6}	0.2588×10^{0}
8	180	2.7223×10^{-5}	3.0724×10^{0}
40		8.5245×10^{-6}	1.9501×10^{0}
90		3.6648×10^{-6}	0.7638×10^{0}
120		2.3972×10^{-6}	0.4799×10^{0}
140		1.8634×10^{-6}	0.3672×10^{0}
170		1.3323×10^{-6}	0.2588×10^{0}
8	270	2.7223×10^{-5}	3.0724×10^{0}
40		8.5245×10^{-6}	1.9501×10^{0}
90		3.6648×10^{-6}	0.7638×10^{0}
110		2.5414×10^{-6}	0.53064×10^{0}
112		2.3958×10^{-6}	0.50554×10^{0}
115		2.1869×10^{-6}	0.470165×10^{0}
120		1.8754×10^{-6}	0.4150×10^{0}
140		1.0753×10^{-6}	0.2561×10^{0}
170		5.2678×10^{-7}	0.14473×10^{0}
Plane z = 80 cm			
0	0, 90, 180	7.1080×10^{-6}	2.1562×10^{0}
4		8.7977×10^{-6}	2.0483×10^{0}
8		1.0518×10^{-5}	1.8150×10^{0}
14		1.5367×10^{-5}	1.5658×10^{0}
20		1.5339×10^{-5}	1.4976×10^{0}
30		1.6303×10^{-5}	1.4908×10^{0}
40		1.5119×10^{-5}	1.3958×10^{0}
50		5.9437×10^{-6}	1.2474×10^{0}

Table 7 (contd)

Coordinates		Radiation intensity	
Radius, cm	Angle, deg	Gamma dose rate, rad/h-thW	Neutron flux, neutrons/cm^2-s-thW
Plane z = 80 cm (contd)			
60		4.8329×10^{-6}	1.0875×10^{0}
70		4.1842×10^{-6}	0.9345×10^{0}
80		3.6528×10^{-6}	0.8000×10^{0}
90		3.1973×10^{-6}	0.6865×10^{0}
100		2.8032×10^{-6}	0.5920×10^{0}
110		2.4662×10^{-6}	0.5134×10^{0}
Plane z = 90 cm			
0	0, 90, 180	3.972×10^{-6}	1.2996×10^{0}
4		4.9802×10^{-6}	1.3136×10^{0}
8		5.6163×10^{-6}	1.2116×10^{0}
14		7.2353×10^{-6}	1.0518×10^{0}
20		9.9609×10^{-6}	0.9968×10^{0}
30		9.6243×10^{-6}	1.0208×10^{0}
40		1.0041×10^{-5}	1.0133×10^{0}
50		9.5751×10^{-6}	0.9555×10^{0}
60		5.84×10^{-6}	0.8703×10^{0}
70		3.5583×10^{-6}	0.7788×10^{0}
80		3.1204×10^{-6}	0.6893×10^{0}
90		2.7692×10^{-6}	0.6069×10^{0}
100		2.4707×10^{-6}	0.5337×10^{0}
110		2.2081×10^{-6}	0.4698×10^{0}
Plane z = 100 cm			
0	0, 90, 180	2.5163×10^{-6}	0.8555×10^{0}
8		3.584×10^{-6}	0.8684×10^{0}
12		3.9454×10^{-6}	0.7968×10^{0}
16		4.5877×10^{-6}	0.7382×10^{0}
20		5.4028×10^{-6}	0.7162×10^{0}
26		5.7691×10^{-6}	0.7135×10^{0}
32		6.1477×10^{-6}	0.7332×10^{0}
40		6.6724×10^{-6}	0.7488×10^{0}
50		6.8636×10^{-6}	0.7371×10^{0}
60		6.631×10^{-6}	0.6978×10^{0}
65		6.4218×10^{-6}	0.6715×10^{0}
70		6.1796×10^{-6}	0.6434×10^{0}
80		2.8784×10^{-6}	0.5855×10^{0}
100		2.1787×10^{-6}	0.4747×10^{0}
120		1.7813×10^{-6}	0.3808×10^{0}
140		1.4697×10^{-6}	0.3074×10^{0}
150		1.3387×10^{-6}	0.2773×10^{0}
160		1.2214×10^{-6}	0.2510×10^{0}
Plane z = 120 cm			
0	0, 90, 180	1.2851×10^{-6}	0.4489×10^{0}
8		1.8344×10^{-6}	0.5056×10^{0}
12		1.9465×10^{-6}	0.4766×10^{0}
16		2.0715×10^{-6}	0.4439×10^{0}
20		2.322×10^{-6}	0.4255×10^{0}
26		2.7318×10^{-6}	0.4156×10^{0}
32		3.3609×10^{-6}	0.4208×10^{0}
40		3.1996×10^{-6}	0.4363×10^{0}

Coordinates		Radiation intensity	
Radius, cm	Angle, deg	Gamma dose rate, rad/h-thW	Neutron flux, neutrons/cm^2-s-thW
Plane z = 120 cm contd			
50		3.5633×10^{-6}	0.4527×10^{0}
60		3.7798×10^{-6}	0.4529×10^{0}
80		3.7395×10^{-6}	0.4200×10^{0}
100		2.9661×10^{-6}	0.36616×10^{0}
105		2.0363×10^{-6}	0.3522×10^{0}
110		1.6969×10^{-6}	0.3385×10^{0}
120		1.4618×10^{-6}	0.31186×10^{0}
140		1.2307×10^{-6}	0.2630×10^{0}
150		1.1357×10^{-6}	0.2414×10^{0}
160		1.0505×10^{-6}	0.2216×10^{0}
Plane z = 40 cm			
0	0	1.9150×10^{-2}	1.2553×10^{2}
4		6.7656×10^{-4}	1.0496×10^{2}
8		1.778×10^{-4}	3.9583×10^{1}
Plane z = 33 cm			
0	0	3.6487×10^{-2}	1.47812×10^{2}
4		1.1377×10^{-3}	1.1820×10^{2}
8		1.8537×10^{-4}	4.2457×10^{1}
Plane z = 150 cm			
0	0, 90, 180	6.3804×10^{-7}	0.2223×10^{0}
4		7.1617×10^{-7}	0.2524×10^{0}
8		8.5432×10^{-7}	0.266×10^{0}
12		9.3657×10^{-7}	0.26425×10^{0}
15		9.6814×10^{-7}	0.2538×10^{0}
25		1.0963×10^{-6}	0.2328×10^{0}
35		1.3393×10^{-6}	0.2280×10^{0}
40		1.5208×10^{-6}	0.2319×10^{0}
65		1.8059×10^{-6}	0.2558×10^{0}
90		2.0224×10^{-6}	0.2535×10^{0}
120		1.9367×10^{-6}	0.2247×10^{0}
140		1.7374×10^{-6}	0.2005×10^{0}
150		1.0535×10^{-6}	0.1887×10^{0}
155		9.3311×10^{-7}	0.1829×10^{0}
170		7.9048×10^{-7}	0.1662×10^{0}
0	263° 33′ 7″	6.3804×10^{-7}	0.2223×10^{0}
4		7.1626×10^{-7}	0.2521×10^{0}
8		8.5661×10^{-7}	0.2642×10^{0}
25		1.1078×10^{-6}	0.2338×10^{0}
35		1.3393×10^{-6}	0.2280×10^{0}
40		1.5215×10^{-6}	0.2317×10^{0}
65		1.8024×10^{-6}	0.2555×10^{0}
90		2.0118×10^{-6}	0.2530×10^{0}
120		1.9271×10^{-6}	0.2242×10^{0}
140		1.4831×10^{-6}	0.2002×10^{0}
150		1.1441×10^{-6}	0.18838×10^{0}
155		9.7853×10^{-7}	0.18266×10^{0}
170		7.9653×10^{-7}	0.16601×10^{0}

Nomenclature

B_i buildup factor for i^{th} energy group at X_i attenuation mean free paths

D_α neutron dose rate at detector point due to each (l,m,n) source point

$D_{u\gamma_i}$ detector response without buildup (uncollided dose rate or appropriate flux term)

D_{γ_i} total dose rate or appropriate flux term at detector

E_i source strength of i^{th} energy group

h composition of material m_o

K_i suitable conversion factor, rad/h/MeV/cm^2-s

l,m,n source points

S volume weighted associated with each (l,m,n) source point, W

$S_{l,m,n}$ volume weighted power associated with each (l, m, n) source point to detector, W

X_{m_o} ratio of hydrogen density in material m_o to that in water

$\alpha_1,\alpha_2,\alpha_3,\alpha_4$ empirical constants fitted to experimental data

$\beta_0,\beta_1,\beta_2,\beta_3$ energy-dependent coefficients provided as input, which are obtained from polynomial fits to buildup data

$\theta_{m_o h}$ fractional density of material m_o in composition h

ρ_h path length through h^{th} composition along source-detector line $\rho_{S_{l,m,n}}$, cm

$\rho_{S_{l,m,n}}$ line-of-sight distance from each (l,m,n) source point to detector, cm

Σ_{m_o} single-energy neutron macroscopic removal cross section

$\Sigma_{m_o i}$ macroscopic gamma attenuation coefficient of material m_o for i^{th} energy group

References

1. Stoddard, D. H., and Albenesius, E. L., *Radiation Properties of ^{238}Pu Produced for Isotopic Power Generators,* DP-984. U.S. Atomic Energy Commission, Washington, D.C., July 1964.
2. Chapman, G. T., and Storrs, C. L., *Effective Neutron Removal Cross Sections for Shielding,* AECD 3978. Oak Ridge National Laboratory, Tenn., Sept. 19, 1955.